Water-resistive and wearable triboelectric nanogenerators based on polyurethane/polyester textiles fabricated utilizing a planarization layer Ⓕ

Ⓘ Young Pyo Jeon, Hak Ji Lee, Young Joon Yoo, et al.

COLLECTIONS

Ⓕ This paper was selected as Featured

View Online   Export Citation   CrossMark

ARTICLES YOU MAY BE INTERESTED IN

Healthcare management applications based on triboelectric nanogenerators
APL Materials 9, 060703 (2021); https://doi.org/10.1063/5.0052605

Pushing the limits of magnetocaloric high-entropy alloys
APL Materials 9, 080702 (2021); https://doi.org/10.1063/5.0058388

Bulk dissipation in the quantum anomalous Hall effect
APL Materials 9, 081116 (2021); https://doi.org/10.1063/5.0056796

Water-resistive and wearable triboelectric nanogenerators based on polyurethane/polyester textiles fabricated utilizing a planarization layer Ⓕ

Young Pyo Jeon,[1] ⓘD Hak Ji Lee,[1] Young Joon Yoo,[1] Keon-Ho Yoo,[2] ⓘD Sang Yoon Park,[1] ⓘD
and Tae Whan Kim[3,a] ⓘD

AFFILIATIONS

[1] Center for Applied Electromagnetic Research for Advanced Institute of Convergence Technology, Seoul National University, Suwon 16229, South Korea
[2] Department of Physics and Research Institute for Basic Sciences, Kyung Hee University, Seoul 02447, South Korea
[3] Department of Electronics and Computer Engineering, Hanyang University, Seoul 04763, South Korea

[a] Author to whom correspondence should be addressed: twk@hanyang.ac.kr

ABSTRACT

We report a water-resistive and wearable triboelectric nanogenerator on a polyurethane/polyester textile substrate with a planarization layer. The power generation and reliability of the triboelectric nanogenerators (TENGs) fabricated utilizing a resin planarization layer were significantly enhanced in comparison with those of TENGs without the resin planarization layer. The planarization layer was deposited on the polyurethane/polyester textile substrate by using spin coating and ultraviolet curing to improve its surface properties and polarity. The output voltages and currents of TENGs based on a resin planarization layer on a polyurethane/polyester substrate were measured in the vertical contact-separation mode by using a counter unit containing Al electrodes and a polyimide friction layer. The TENGs exhibited a peak potential of over 30 V, which is about three times larger than that of the devices without such a planarization layer, and the corresponding maximum power density was 3.16 mW/m^2. Furthermore, the results of endurance and water resistance tests carried out on the TENGs with a resin planarization layer on a textile substrate showed that such devices were suitable for use in applications in which the device must be worn.

I. INTRODUCTION

Textile-based electronic devices have attracted extraordinary attention for next-generation electronic applications due to their excellent material advantages of flexibility, light weight, and versatility, their excellent physical properties when used in thin devices, and their durability under tension and high humidity.[1–6] Wearable devices, as represented by smart mobile applications, is a field that is greatly influenced by the development of textile-based electronic devices. Recently, much research has been conducted on wearable electric devices to reduce their power consumption, size, and weight and to integrate several functions into the textile system.[7–14] As a result of various research efforts, the performance of wearable devices has evolved in many ways, but in order for more practical wearable devices to be developed, the need for a plug-in power supply must be eliminated.[15–18] The power source for currently available wearable devices is a conventional capacitor-based battery, which has a limited lifetime and must have a large size so as to achieve a sufficiently large capacitance. Alternatively, flexible, transparent, and stretchable batteries suffer from low mechanical durability and short battery lifetimes.[19–21]

Triboelectric nanogenerators (TENGs) use renewable energy-harvesting technology based on the electric polarity difference between two active layers. The major principle underlying the energy-harvesting mechanism of TENGs is the conversion of mechanical energy into electricity.[22–28] Hence, the major advantage of TENGs, when compared with other renewable energy-harvesting candidates, such as those based on photovoltaic, tidal, and wind

electricity generation, is the fact that they can be operated independently of solar, wave, and wind power.[29–33] In particular, because of the ability of TENGs to generate electricity independent of the environment, wearable TENGs (WTENGs) have been widely studied and have become attractive candidates for use as power sources in plug-in-free devices and simple mobile electronics. Recently, some promising research results on enhancing the efficiency of highly reliable TENGs fabricated using simple processes and capable of continuously generating energy have been reported.[34–38]

One of the most attempted ways to realize highly efficient TENGs with enhanced power generation is the use of nanostructures, such as nano-rods, nano-particles, and nano-ripples, to increase the difference in the polarities and contact area.[27,28] In the case of WTENGs, because the textile substrate has a certain pattern and may not be even, the very weak adhesion between the textile and the nanostructure, which might cause mechanical durability issues, must be overcome.[39–41] One way to overcome the weak adhesion is to employ a stacked layer that covers the pattern of the textile substrate.[42–45]

In this paper, we present WTENGs based on a polyurethane/polyester textile substrate with a resin planarization layer. As the planarization layer, a UV-cured resin was deposited onto the polyurethane/polyester textile substrate to improve its morphology and polarity. TENGs with various polymeric materials have been studied; however, TENGs with the resin planarization layer, consisted of mercapto ester and triallyl isocyanurate, have some advantages for higher power generation and surface protectivity. Scanning electron microscopy (SEM) images showed the surface conditions of the textile substrates with and without a resin planarization layer. The output voltage and current of the TENGs based on a planarized textile substrate containing Ag electrodes and a polyimide friction layer and operating in the vertical contact-separation mode were measured, and a peak potential of over 30 V, which is about three times larger than that of the device without the resin planarization layer, was realized. Furthermore, endurance tests were performed over 500 cycles of the TENG based on the textile substrate with a resin planarization layer operating in the vertical-contact

mode; moreover, the water resistance property was tested after the TENG had been soaked for 30 min in water. The results confirmed that our device, which was fabricated using a simple and low-cost process, is suitable for use in plug-in-free and wearable electronic devices.

II. EXPERIMENTAL DETAILS

Polyester/polyurethane textile substrates were cut into squares of $(2.5 \text{ cm})^2$, and N_2 gas with a purity of 99.999% was blown over them to remove any dust and liquid. The cleaned textile substrate was attached to bare glass for ease of handling during the deposition of the resin onto the textile substrate. The resin, which is produced by Norland Products, Inc., is called Norland Optical Adhesive 63. The triboelectric series of the resin have not been revealed, but it might be more positive than those of Kapton and DuraLar polyester film considering the triboelectric series of polymeric epoxy resin agents.[46,47] We spin-coated the resin onto the textile substrate at 2000 rpm for 35 s, after which we allowed the textile substrates to stand for 10 min. Then, the textile substrates were exposed to 365-nm light from a UV lamp (6 W, Vilber Lourmat, 230 V, 50/60 Hz) for 2 h to cure the resin. The textile substrate with the UV-treated resin coating was loaded into a vacuum chamber, and a 100-nm Ag electrode was deposited onto it. The entire fabrication process for the conductive, wearable, textile substrate is pictorially illustrated in Figs. 1(a)–1(g); a photograph of a TENG with a resin/polyester/polyurethane textile substrate attached to a shirt is shown on the right side of the figure. The counter electrode was an Al foil attached to a polyimide film called Kapton.

Scanning electron microscope (SEM) images of the surfaces of the Ag/polyester/polyurethane textile substrates with and without the resin planarization layer were obtained by using a Nova Nano SEM 200 system operating at 15 kV; the scanning area was $15 \times 15 \text{ mm}^2$ and was viewed with 100 times magnification. The contact-angle for deionized water was obtained by a contact-angle measuring instrument (Phoenix 300 A, SEO Co., Inc.). The mechanical properties of the textile substrates without and with a resin
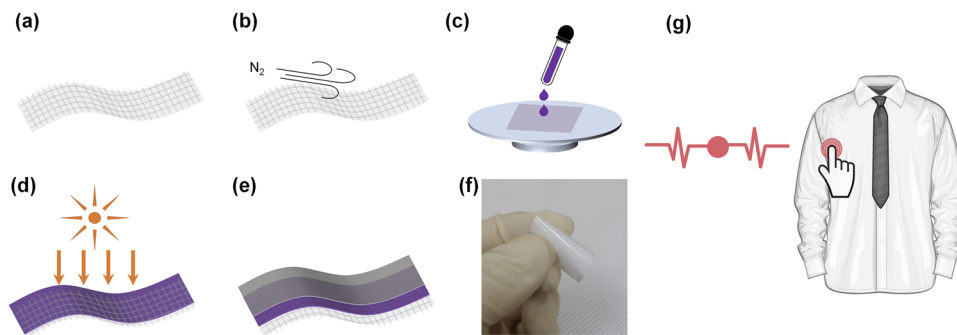

FIG. 1. Schematic diagram for the production of a triboelectric nanogenerator (TENG) based on a polyester/polyurethane textile substrate. (a) The polyester/polyurethane textile substrate was cut into squares with an area of $2.5 \times 2.5 \text{ cm}^2$. (b) Nitrogen gas with a purity of 99.999% was blown over the polyester/polyurethane textile substrate to clean its surface and pores. (c) A resin layer was spin-coated onto the polyester/polyurethane textile substrate. (d) The polyester/polyurethane textile substrate was exposed to light from a 365-nm UV lamp. (e) An Ag electrode was evaporated onto the resin/polyester/polyurethane textile substrate. (f) A photograph of the completed wearable TENG. (g) The wearable TENG can be operated by tapping on clothes to generate electricity.
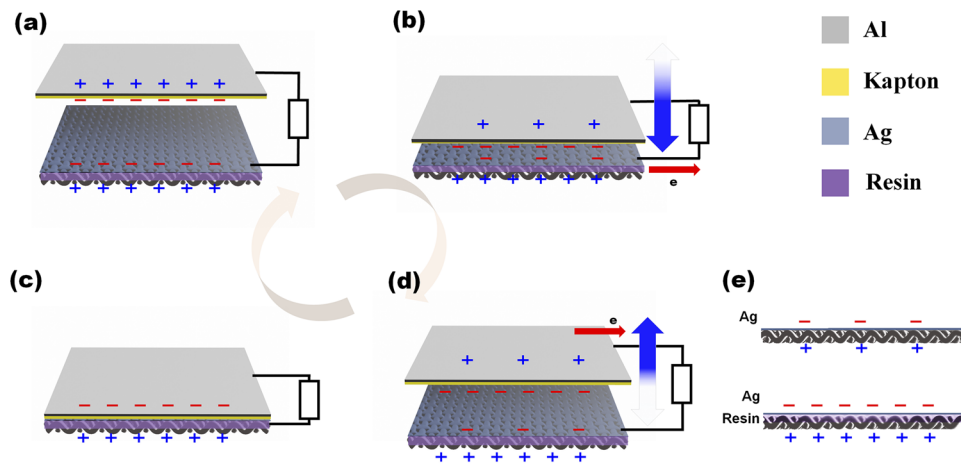
FIG. 2. (a)–(d) Schematic illustrations for one cycle of a triboelectric nanogenerator (TENG) operating in the contact-separation mode and (e) the comparison between the surface morphology and the adhesion to the Ag electrode without and with a resin planarization layer. The electron flow due to the movements of electrons and holes during the operation of the TENG is graphically shown.

planarization layer were measured using a universal testing machine (UTM, LR5KPlus, LLOYD Instruments Ltd.) with a loading rate of 1 mm/min. A handmade TENG measurement system integrated with a four-channel digital storage oscilloscope (TDS 2024C, 200 MHz/2 GS/s, Tektronix) was used to measure the open-circuit voltage of the TENGs while being worn and operating in the vertical contact-separation mode with tapping as the power source. The output voltage performance of a wearable triboelectric nanogenerator attached to a cotton sheet operating in the single-electrode mode and sliding mode with water droplets were also measured. The short-circuit current and the endurance of the output voltages for the TENGs after having been washed were measured using a DMM7510 7 1/2-digit multimeter (Keithley), which is a four-channel electrometer with an inner impedance of 10 Ω.
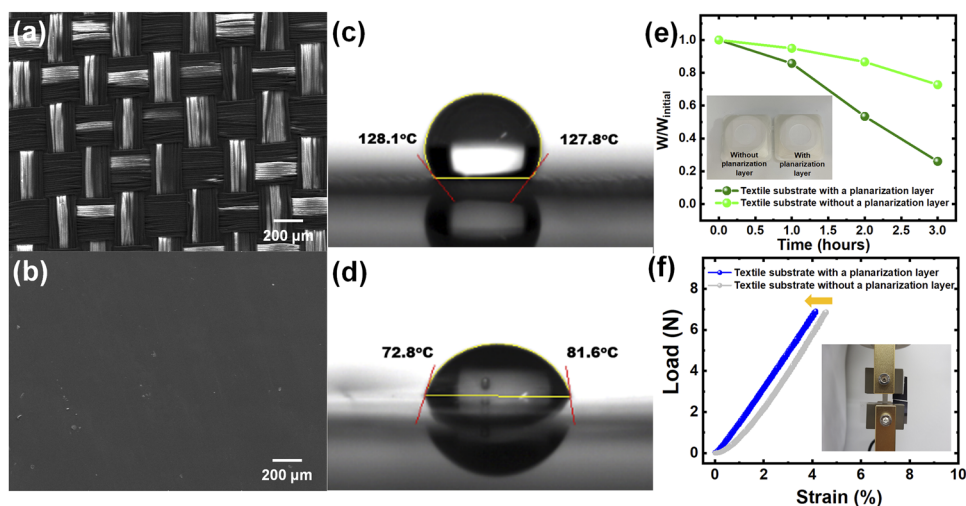

FIG. 3. Scanning electron microscopy images of the surfaces of the polyester/polyurethane textile substrates (a) without and (b) with a resin planarization layer. The images are magnified 100 times, and scale bars are included. The contact-angle for water of the polyester/polyurethane textile substrates (c) without and (d) with a resin planarization layer. (e) Breathability of the textile substrates without and with a resin planarization layer in the sealed container at 45 °C for 3 h. (f) The inserted image of the universal testing machine (UTM) measurement performing the textile substrate of 2×0.5 cm^2 and load–strain curves of the textile substrate without and with a resin planarization layer.

III. RESULTS AND DISCUSSION

Figures 2(a)–2(d) illustrate the operation of the textile-based TENGs operating in the vertical contact-separation mode. The triboelectricity in both friction layers (Kapton and textile substrate) causes the electrons in both electrodes to relocate as a result of the contact and separation. The triboelectric difference between the friction layers greatly affects the movement of electrons to the opposite electrode in order to achieve electrical equilibrium in the device, as has been reported in various papers.[24,31] The performance of a TENG also depends very much on the materials used and their surface conditions because voltage generation in a TENG is the result of actual electron exchange between the negative and the positive friction layers. Because of this, a resin planarization layer should improve the surface morphology and the adhesion to the Ag electrode, which is crucial for increasing the efficiencies and reliabilities of TENGs based on textile substrates [Fig. 2(e)].

Figures 3(a) and 3(b) show SEM images of Ag/polyester/ polyurethane textile substrates without and with the resin planarization layer, respectively. The morphologies of the textile substrate were significantly changed by the resin planarization layer. While the surface of the Ag/polyester/polyurethane textile substrate was uneven due to their bare fabric structure of the polyester/polyurethane, that of the planarized substrate was sufficiently flat. The contact-angle for water was indicative of the surface roughness of the textile substrates without and with the resin planarization layer [Figs. 3(c) and 3(d)]. The surface of the textile substrate with the planarization layer shows greater water-droplet dispersion than that without the planarization layer as the surface becomes smoother.

To quantitatively evaluate the breathability of our textile, the mass change of the water in the sealed container covering the opening of the textile substrate without and with a resin planarization layer is observed, as shown in Fig. 3(e). The temperature around the
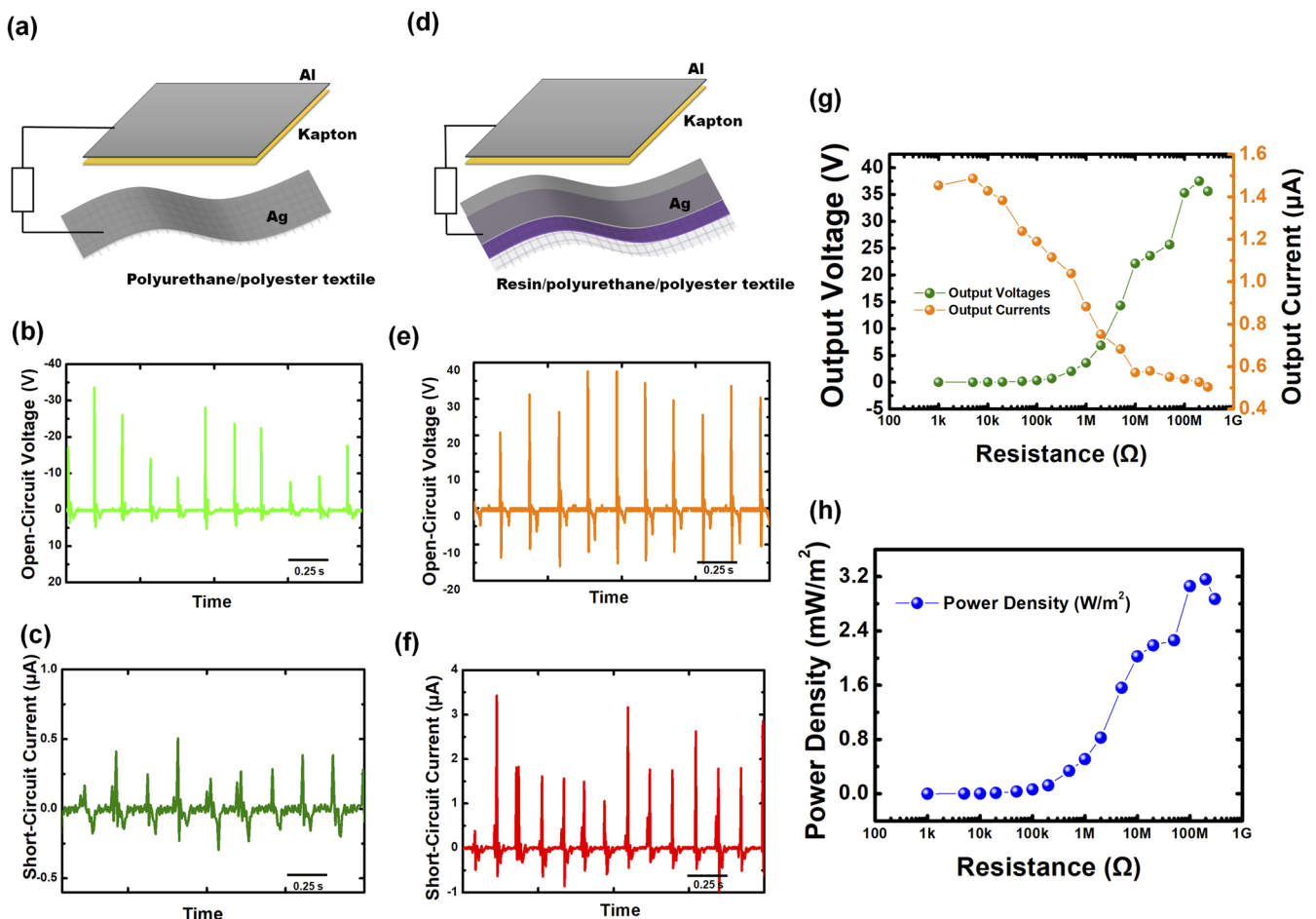

FIG. 4. Enhanced electrical performance of a triboelectric nanogenerator (TENG) with a planarization layer. Graphical structures of the TENGs (a) without and (d) with a resin planarization layer for operation in the vertical contact-separation mode. (b) and (e) Open-circuit voltages and (c) and (f) short-circuit currents of TENGs with Ag/polyester/polyurethane and with Ag/resin/polyester/polyurethane substrates, respectively, for operation in the vertical contact-separation mode (4 Hz). (g) Dependences of the output voltages and the output currents of the TENGs with a Ag/resin/polyester/polyurethane structure on the load resistance for resistances from 1 kΩ to 300 MΩ. (h) Power density of the TENG as a function of the resistance, as calculated by using the output voltage and the output current for an active area of $(2.5 \text{ cm})^2$.

sealed container was controlled at ~45 °C for 3 h. The mass of the water in the sealed containers covering the textile substrate without and with a resin planarization layer were reduced by 74% and 28%. The water evaporation ratios of the textile substrate without and with a resin planarization layer were 0.012 and 0.004 kg m^{-2} h^{-1}, respectively. Figure 3(f) shows the load–strain curves of the textile substrate without and with a resin planarization layer. The textile substrate without a resin planarization layer exhibits stretchability with elongation up to 4.57% at 7 N, which is slightly higher than that of the textile substrate with a resin layer of 4.11% at the same force. Overall, the stacked resin planarization layer does not adversely affect its breathability and ductile property of the textile substrate.

In order to contrast the electrical performance of the TENGs with and without the resin planarization layer, we measured the open-circuit voltages and short-circuit currents of TENGs operating in the vertical contact-separation mode by tapping, and the results are shown in Fig. 4. The peak open-circuit voltage and short-circuit current of the TENGs with the resin planarization layer were about 30 V and 2 μA, respectively, much higher than those of the TENGs without the resin planarization layer, indicative of enhanced triboelectric power generation due to the presence of the resin planarization layer [Figs. 4(b)–4(f)]. Antisymmetric performances in the positive and negative regions were observed in the open-circuit voltages and short-circuit currents of the TENGs, which were caused by the use of a tapping measurement system. Moreover, the direct contact between the upper dielectric layer and the Ag electrode can afford the charge generation of the device, making in the negative voltages of our TENGs being mostly smaller than the positive voltages. However, the resin planarization layer, whose triboelectric series is more positive than that of the textile, compensates the charge generation process because the increment in the negative voltage of the TENG with the resin planarization layer is greater than that of the positive voltage.

The dependences of the output voltage and the output current of the TENGs with a Ag/resin/polyester/polyurethane structure on the load resistance were measured, and the results are shown in Fig. 4(g). The load resistance was varied from 1 kΩ to 300 MΩ. In this resistance range, the voltage increased with the increasing load resistance and gradually saturated at resistances above 100 MΩ, while the output current decreased from 1.5 to 0.5 μA. Consequently, the power density increased from 0.266 μW/m^2 to a maximum of 3.16 mW/m^2 at a load resistance of 200 MΩ [Fig. 4(h)].

The endurance tests of the textile TENGs were conducted at room temperature, and the results are shown in Fig. 5(a). The open-circuit voltage experienced no noticeable degradation during 500 repetitive operations, indicating that the performances of the TENGs were very stable. Because WTENGs should be water resistant, we tested the water resistance of a Ag/resin/polyester/polyurethane unit (2.5 × 2.5 cm^2) by totally submerging it in water at 20 °C for 30 min, which is a possible laundering condition, and the results are shown in Fig. 5(b). The unit was naturally dried for 3 h to restore it to its original state; then, the open-circuit voltage was measured. The open-circuit voltage of the washed TENG, which is shown in Fig. 5(c), was slightly lower than that of the unwashed TENG [Fig. 5(a)], and its endurance was less stable with a marginally increased noise. These results are thought to be due to the presence of remaining water, which disrupts the flow of electricity.

In order to prove that out TENGs are suitable for use as wearable devices, we obtained the electric performances of the TENGs operating in the single-electrode mode [Fig. 6(a)], and the results are shown in Figs. 6(b) and 6(c). The WTENG was designed to have a structure similar to that of a device attached to the inside of cotton clothes. The peak open-circuit voltage and short-circuit current were about 2 V and 0.4 μA through ten cycles of operation. Their efficiency and reliability when operated in the single-electrode mode were remarkably different from those in the vertical
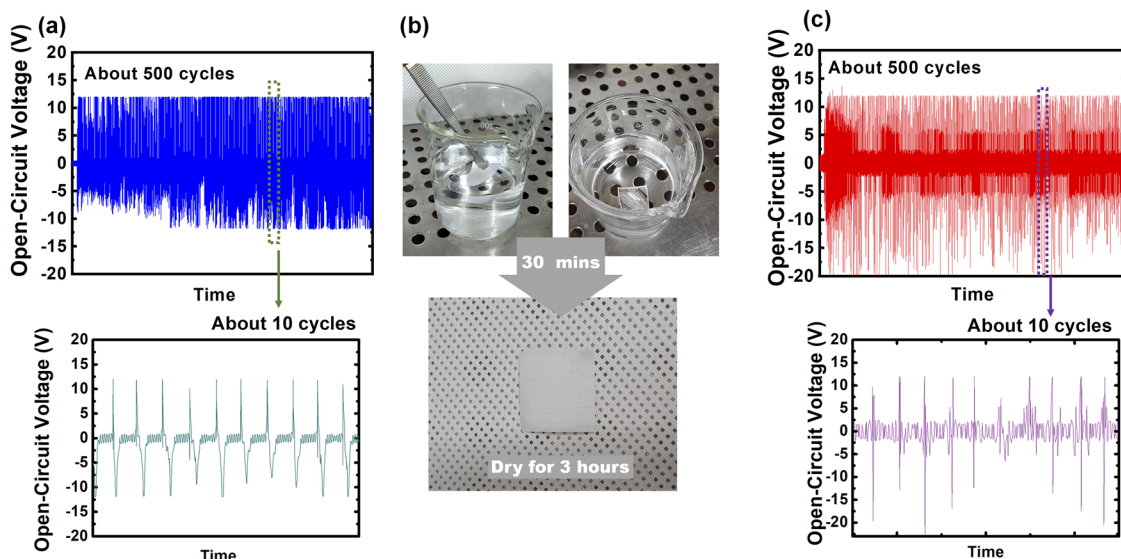

FIG. 5. Endurance and water resistance of TENGs with Ag/resin/polyester/polyurethane textile substrates. (a) Endurance of the open-circuit voltage during repetitive operations of about 500 cycles, including an enlarged view for the ten cycles in the middle. (b) For cleaning, we allowed the Ag/resin/polyester/polyurethane textile substrate to remain under water for 30 min, after which it was naturally dried for 3 h. (c) To determine the water resistance, we measured the open-circuit voltage of a TENG with a washed Ag/resin/polyester/polyurethane textile substrate during repetitive operations of about 500 cycles.
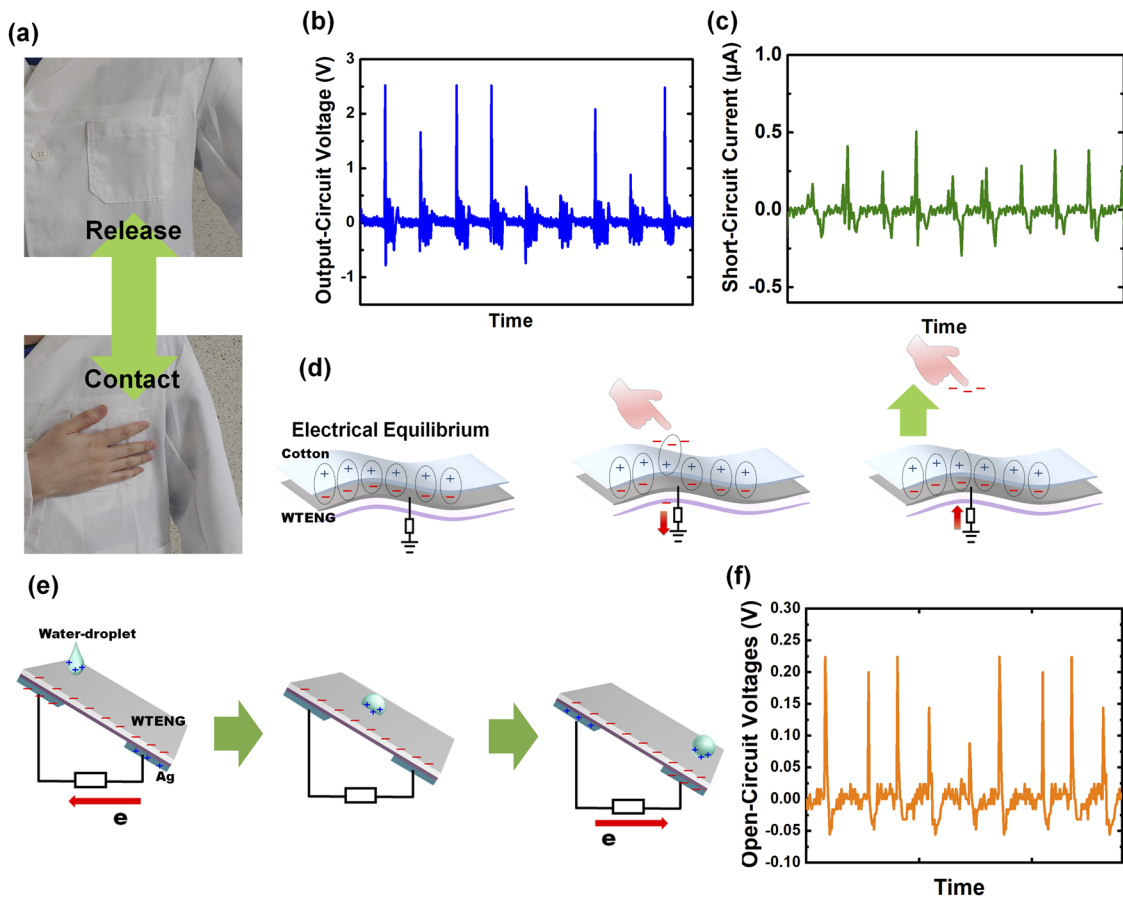
FIG. 6. (a) An example for the WTENG used as a wearable device operating in the single-electrode mode. (b) Open-circuit voltage and (c) short-circuit current as functions of time, along with (d) schematic illustrations for one operating cycle for a WTENG operated in the single-electrode mode by using a human finger. (e) Schematic diagram and (f) the open-circuit voltage of the WTENG collecting energy from water droplets.

contact-separation mode because the counter unit of the TENG was the human body and the human body is not electrically stable due to the atmosphere. The operation mechanism for a TENG in the single-electrode mode is shown in Fig. 6(d). In detail, the electric charge of the cotton, the Ag electrode, and the grounded electrical load was balanced, and the approaching human body broke the electrical equilibrium, thus allowing the electrons to move. As the human body moves away from the device, electrons may be restored and equilibrium may be re-established because no actual electron exchange occurs between the human body and the Ag electrode.

Moreover, we performed the electric performances of the WTENGs to collect energy from dropping aqua droplets. According to the working mechanism as mentioned above, the electron transfer and electricity generation are mainly driven by the triboelectrification and the electrostatic induction processes, as shown in Fig. 6(e). The height and the inclination angle were simply fixed to 10 cm and 50°, respectively. The maximum open-circuit voltage of the WTENG from a dropping aqua droplet was 0.22 V, as shown in Fig. 6(f), and the triboelectric energy of the WTENG was continuously collected by the flowing aqua droplet, thus causing a change in

the electrostatics between the water droplet and the textile substrate with a resin planarization layer.

IV. CONCLUSION

In summary, we fabricated a water-resistive and wearable TENG using a polyurethane/polyester textile substrate. A resin planarization layer was purposely deposited onto the polyurethane/polyester textile substrate to increase both the amount of electricity generated and the reliability of the device. The measured open-circuit voltage and short-circuit current for the TENG with a resin planarization layer operating in the vertical contact-separation mode were significantly increased in comparison with those for the TENG without the planarization layer. The output voltage increased gradually with increasing load resistance, and a maximum power density of 3.16 mW/m² was achieved at a load resistance of 200 MΩ. The measured endurance and water resistance of the TENG with the resin planarization layer confirmed its suitability for use in a water-resistive and wearable device. The electrical performances of TENGs operated in the single-electrode mode by using

the human body and working from moving droplets were measured, and the peak open-circuit voltages were about 2 and 0.22 V, respectively, during ten cycle operations, further confirming its suitability for use in practical applications.

ACKNOWLEDGMENTS

DATA AVAILABILITY

The data that support the findings of this study are available from the corresponding author upon reasonable request.

REFERENCES

[1] J. S. Heo, J. Eom, Y.-H. Kim, and S. K. Park, Small **14**, 1703034 (2018).

[2] Z. Tian, J. He, X. Chen, Z. Zhang, T. Wen, C. Zhai, J. Han, J. Mu, X. Hou, X. Chou, and C. Xue, Nano Energy **39**, 562–570 (2017).

[3] Q. Huang, D. Wang, and Z. Zheng, Adv. Energy Mater. **6**, 1600783 (2016).

[4] J. Lv, I. Jeerapan, F. Tehrani, L. Yin, C. A. Silva-Lopez, J.-H. Jang, D. Joshuia, R. Shah, Y. Liang, L. Xie, F. Soto, C. Chen, E. Karshalev, C. Kong, Z. Yang, and J. Wang, Energy Environ. Sci. **11**, 3431–3442 (2018).

[5] Z. Chai, N. Zhang, P. Sun, Y. Huang, C. Zhao, H. J. Fan, X. Fan, and W. Mai, ACS Nano **10**, 9201–9207 (2016).

[6] M. Parrilla, R. Cánovas, I. Jeerapan, F. J. Andrade, and J. Wang, Adv. Healthcare Mater. **5**, 996–1001 (2016).

[7] H. Park, J. W. Kim, S. Y. Hong, G. Lee, H. Lee, C. Song, K. Keum, Y. R. Jeong, S. W. Jin, D. S. Kim, and J. S. Ha, ACS Nano **13**, 10469–10480 (2019).

[8] Y. Zhong, Y. Xia, W. Mai, J. Tu, and H. J. Fan, Adv. Mater. Technol. **2**, 1700182 (2017).

[9] L. Dong, G. Liang, C. Xu, W. Liu, Z.-Z. Pan, E. Zhou, F. Kang, and Q.-H. Yang, Nano Energy **34**, 242–248 (2017).

[10] X. Pu, W. Hu, and Z. L. Wang, Small **14**, 1702817 (2018).

[11] S. Li, Y. Fan, H. Chen, J. Nie, Y. Liang, X. Tao, J. Zhang, X. Chen, E. Fu, and Z. L. Wang, Energy Environ. Sci. **13**, 896–907 (2020).

[12] J. Nie, Z. Ren, L. Xu, S. Lin, F. Zhan, X. Chen, and Z. L. Wang, Adv. Mater. **32**, 1905696 (2020).

[13] Y. Shi, F. Wang, J. Tian, S. Li, E. Fu, J. Nie, R. Lei, Y. Ding, X. Chen, and Z. L. Wang, Sci. Adv. **7**, eabe2943 (2021).

[14] K. Liu, Y. Yao, T. Lv, H. Li, N. Li, Z. Chen, G. Qian, and T. Chen, J. Power Sources **446**, 227355 (2020).

[15] H. Chu, H. Jang, Y. Lee, Y. Chae, and J.-H. Ahn, Nano Energy **27**, 298–305 (2016).

[16] Y. Wang and Y. Yang, Nano Energy **56**, 547–554 (2019).

[17] J. Deng, X. Kuang, R. Liu, W. Ding, A. C. Wang, Y.-C. Lai, K. Dong, Z. Wen, Y. Wang, L. Wang, H. J. Qi, T. Zhang, and Z. L. Wang, Adv. Mater. **30**, 1705918 (2018).

[18] D. Shen, M. Xiao, G. Zou, L. Liu, W. W. Duley, and Y. N. Zhou, Adv. Mater. **30**, 1705925 (2018).

[19] J. Liu, M. Hu, J. Wang, N. Nie, Y. Wang, Y. Wang, J. Zhang, and Y. Huang, Nano Energy **58**, 338–346 (2019).

[20] J. Zhao, K. K. Sonigara, J. Li, J. Zhang, B. Chen, J. Zhang, S. S. Soni, X. Zhou, G. Cui, and L. Chen, Angew. Chem. **129**, 7979 (2017).

[21] Q. Li and H. Ardebili, J. Power Sources **303**, 17–21 (2016).

[22] X. He, H. Zou, Z. Geng, X. Wang, W. Ding, F. Hu, Y. Zi, C. Xu, S. L. Zhang, H. Yu, M. Xu, W. Zhang, C. Lu, and Z. L. Wang, Adv. Funct. Mater. **28**, 1805540 (2018).

[23] S.-B. Jeon, S.-J. Park, W.-G. Kim, I.-W. Tcho, I.-K. Jin, J.-K. Han, D. Kim, and Y.-K. Choi, Nano Energy **53**, 596–603 (2018).

[24] L. Feng, G. Liu, H. Guo, Q. Tang, X. Pu, J. Chen, X. Wang, Y. Xi, and C. Hu, Nano Energy **47**, 217–223 (2018).

[25] Z. Lin, J. Yang, X. Li, Y. Wu, W. Wei, J. Liu, J. Chen, and J. Yang, Adv. Funct. Mater. **28**, 1704112 (2018).

[26] I. J. Chen, W. Kim, W. Jang, H.-W. Park, A. Sohn, K.-B. Chung, D.-W. Kim, D. Choi, and Y. T. Park, J. Mater. Chem. A **6**, 3108–3115 (2018).

[27] Y. P. Jeon, J. H. Park, and T. W. Kim, Appl. Surf. Sci. **445**, 50–55 (2018).

[28] Y. P. Jeon, J. H. Park, and T. W. Kim, Appl. Surf. Sci. **466**, 210–214 (2019).

[29] S. S. K. Mallineni, Y. Dong, H. Behlow, A. M. Rao, and R. Podila, Adv. Energy Mater. **8**, 1702736 (2018).

[30] Y. Jie, X. Jia, J. Zou, Y. Chen, N. Wang, Z. L. Wang, and X. Cao, Adv. Energy Mater. **8**, 1703133 (2018).

[31] Q. Shi, T. He, and C. Lee, Nano Energy **57**, 851–871 (2019).

[32] Y. Dong, S. S. K. Mallineni, K. Maleski, H. Behlow, V. N. Mochalin, A. M. Rao, Y. Gogotsi, and R. Podila, Nano Energy **44**, 103–110 (2018).

[33] N. P. Maria Joseph Raj, N. R. Alluri, V. Vivekananthan, A. Chandrasekhar, G. Khandelwal, and S.-J. Kim, Appl. Energy **228**, 1767–1776 (2018).

[34] Y. Song, H. Wang, X. Cheng, G. Li, X. Chen, H. Chen, L. Miao, X. Zhang, and H. Zhang, Nano Energy **55**, 29–36 (2019).

[35] H. Wang, J. Wang, T. He, Z. Li, and C. Lee, Nano Energy **63**, 103844 (2019).

[36] J. Wang, H. Wang, N. V. Thakor, and C. Lee, ACS Nano **13**, 3589–3599 (2019).

[37] J. Wang, L. Pan, H. Guo, B. Zhang, R. Zhang, Z. Wu, C. Wu, L. Yang, R. Liao, and Z. L. Wang, "Rational structure optimized hybrid nanogenerator for highly efficient water wave energy harvesting," Adv. Energy Mater. **9**, 1802892 (2019).

[38] Q. Tang, X. Pu, Q. Zeng, H. Yang, J. Li, Y. Wu, H. Guo, Z. Huang, and C. Hu, Nano Energy **66**, 104087 (2019).

[39] P. Howli, K. Panigrahi, A. Mitra, N. S. Das, and K. K. Chattopadhyay, Appl. Surf. Sci. **485**, 238–246 (2019).

[40] S. Xu, D. Cen, P. Gao, H. Tang, and Z. Bao, Nanoscale Res. Lett. **13**, 65 (2018).

[41] F. Nogueira, N. Karumidze, I. Kusradze, M. Goderdzishvili, P. Teixeira, and I. C. Gouveia, Nanomed.: Nanotechnol., Biol. Med. **13**, 2475–2484 (2017).

[42] T. Carey, S. Cacovich, G. Divitini, J. Ren, A. Mansouri, J. M. Kim, C. Wang, C. Ducati, R. Sordan, and F. Torrisi, Nat. Commun. **8**, 1202 (2017).

[43] S. Choi, S. Kwon, H. Kim, W. Kim, J. H. Kwon, M. S. Lim, H. S. Lee, and K. C. Choi, Sci. Rep. **7**, 6424 (2017).

[44] W. Kim, S. Kwon, Y. C. Han, E. Kim, K. C. Choi, S.-H. Kang, and B.-C. Park, Adv. Electron. Mater. **2**, 1600220 (2016).

[45] D. Yin, Z.-Y. Chen, N.-R. Jiang, Y.-F. Liu, Y.-G. Bi, X.-L. Zhang, W. Han, J. Feng, and H.-B. Sun, Org. Electron. **76**, 105494 (2020).

[46] H. Zou, Y. Zhang, L. Guo, P. Wang, X. He, G. Dai, H. Zheng, C. Chen, A. C. Wang, C. Xu, and Z. L. Wang, Nat. Commun. **10**, 1427 (2019).

[47] X. Zhang, L. Chen, Y. Jiang, W. Lim, and S. Soh, Chem. Mater. **31**, 1473–1478 (2019).